ELSEVIER

Earth and Planetary Science Letters 168 (1999) 45–63

EPSL

Variations in the geochemistry of magmatism on the East Pacific Rise at 10°30′N since 800 ka

M. Regelous [a,*], Y. Niu [a], J.I. Wendt [a], R. Batiza [b], A. Greig [a], K.D. Collerson [a]

[a] *Department of Earth Sciences, The University of Queensland, Brisbane, QLD 4072, Australia*
[b] *Department of Geology and Geophysics, University of Hawaii, Honolulu, HI 96822, USA*

Received 21 July 1998; revised version received 29 January 1999; accepted 8 February 1999

Abstract

Samples of volcanic rock, collected from the flanks of the East Pacific Rise at 10°30′N, were used to investigate changes in the geochemistry of magmatism at the ridge axis, over the past 800 ka at this location. We show that there have been large variations in the major element chemistry of the lavas erupted at the spreading axis on this ridge segment over this period. For example, the average MgO content of lavas erupted at the ridge axis increased from about 3.0% at 600 ka, to about 7.0% at 300 ka. Since 300 ka the average MgO content has systematically decreased, and the average MgO content of lavas collected from within the neovolcanic zone at 10°30′N is 6.0%. These temporal changes in major element chemistry are not accompanied by systematic changes in isotope composition or incompatible trace element ratios, and are interpreted to reflect changes in the average rate of supply of melt to the ridge axis during this period. The data support previous arguments that changes in melt supply rate over periods of 100–1000 ka have an important influence on the major element chemistry of the lavas erupted at fast spreading ridges. At 10°30′N, the melt supply rate appears to have been relatively low for much of the past 800 ka. Samples younger than 50 ka, collected from within 3 km of the ridge axis at 10°30′N (inside the neovolcanic zone), have a smaller range in major element chemistry compared to the samples dredged from the ridge flanks. Variations in the chemistry of lavas erupted over periods of less than about 100 ka may be controlled by the geometry of the magma plumbing system beneath the ridge axis.

Keywords: major elements; geochemistry; volcanic rocks; igneous activity; East Pacific Rise; magma chambers

1. Introduction

Recent geophysical studies of the East Pacific Rise (EPR) have provided evidence that an axial magma chamber (AMC) exists beneath many segments of this fast-spreading ocean ridge [1,2]. Magma chambers have an important influence on the chemistry of the lavas that are erupted at the ridge axis [3,4]. For example, convective mixing within the AMC will tend to homogenize melt compositions, and the systematic chemical variations observed in the lavas erupted along several well-studied segments of the EPR may reflect chemically and thermally zoned magma chambers beneath the axis [5,6]. Abrupt changes in mid-ocean ridge basalt (MORB) chemistry often occur across discontinuities in the mid-ocean ridge spreading system such as transform

* Corresponding author. Present address: Max-Planck-Institut für Chemie, Abteilung Geochemie, Postfach 3060, 55020 Mainz, Germany. Fax: +49-6131-371051; E-mail: regelous@mpch-mainz.mpg.de

0012-821X/99/$ – see front matter
PII: S0012-821X(99)00048-5

faults, overlapping spreading centers or devals, suggesting that the magmatic plumbing system beneath the ridge axis may be offset beneath such discontinuities [5,7–10]. Geochemical variations between adjacent ridge segments may also partly reflect differences in the composition of parental magmas that feed different segments [11–13]. Clearly, geochemical studies can give important information on the structure of the magma chambers that exist beneath mid-ocean ridges [14]. However, many aspects of the melt supply process and magma plumbing systems beneath mid-ocean ridges are not well understood. For example, the importance of focussed melt supply to the magma chamber and along-axis flow of melt at crustal levels is not clear, nor is the relationship between tectonic and petrological segmentation of the ridge axis.

Most geochemical studies of mid-ocean ridge magmatism have centered on young lavas recovered from close to active spreading centers, and as a result, very little is known about the temporal variations in the geochemistry of MORB erupted at a single segment of the mid-ocean ridge system. However, a knowledge of how magma chemistry has evolved with time could provide important insights into magma chamber structure and evolution. For example, it is uncertain whether magma chambers are steady-state features, in which melt supply is balanced by melt loss by eruption along each segment of the ridge, or whether the volume, composition, and segmentation of the AMC system varies with time. Several authors have proposed that variations in the magma supply rate and magma chemistry may occur over periods of 10–1000 ka [15–23], but because systematic off-axis sampling has been so limited, the timescales of temporal variations in MORB chemistry, and the processes which control these chemical variations are not well understood.

Most previous studies of off-axis lavas from the flanks of the EPR have been limited to samples collected from within about 10 km of the ridge axis [17,18,20]. In this paper, we present geochemical data for a suite of lavas dredged from up to 50 km from the EPR axis, on each side of the ridge axis (on the Pacific and Cocos Plates, Fig. 1) at 10°30′N. We show that these samples can be used to investigate changes in the chemistry of MORB erupted at the ridge axis over the last ~800 ka. The 10°30′N region of the EPR is an ideal place to study temporal changes in the chemistry of MORB erupted on a single ridge segment, because the structure of this ridge segment is relatively simple, and the along-axis geochemical variation is well known. In addition, this region of the EPR has been the focus of several detailed geological and geophysical studies, which have provided insights into the structure of the crust and the dimensions of magma bodies beneath this ridge segment [24–26].

The samples we have analyzed were studied previously by Batiza et al. [21], who showed that the variation in major element chemistry of lavas dredged from the flanks of the EPR at 10°30′N is much greater than in lavas from the seafloor up to 50 km from the ridge axis at 9°30′N and 11°20′N. Batiza et al. [21] argued that at 9°30′N and 11°20′N, steady-state magma chambers beneath the ridge axis have buffered the compositions of the lavas erupted over the past ~800 ka, whereas at 10°30′N the rate of melt supply has been relatively low over the same period, leading to larger variations in the average temperature and composition of the magma chamber beneath the ridge. In this paper, we report combined major and trace element and Sr, Nd and Pb isotope data for the samples from 10°30′N, in order to examine in more detail temporal variations in the chemistry of the lavas that have been erupted at this location, and to use these chemical variations to constrain the evolution of the AMC system beneath this ridge segment.

2. Tectonics and geochemistry of the EPR at 10°30′N

Samples were collected from along a flowline across the EPR axis at 10°30′N (about 25 km to the north of the Clipperton Fracture Zone), during the Phoenix 02 (R/V *Melville*) expedition. The samples are from 40 dredges from out to a distance of about 50 km from the EPR axis on both the Pacific and Cocos Plates (Fig. 1). The oldest samples were collected from seafloor close to the Matuyama–Brunhes magnetic reversal (about 800 ka). Most samples collected from off-axis were dredged from fault scarps, but closer to the ridge axis, an additional 30 samples were recovered by a rock-coring technique, which

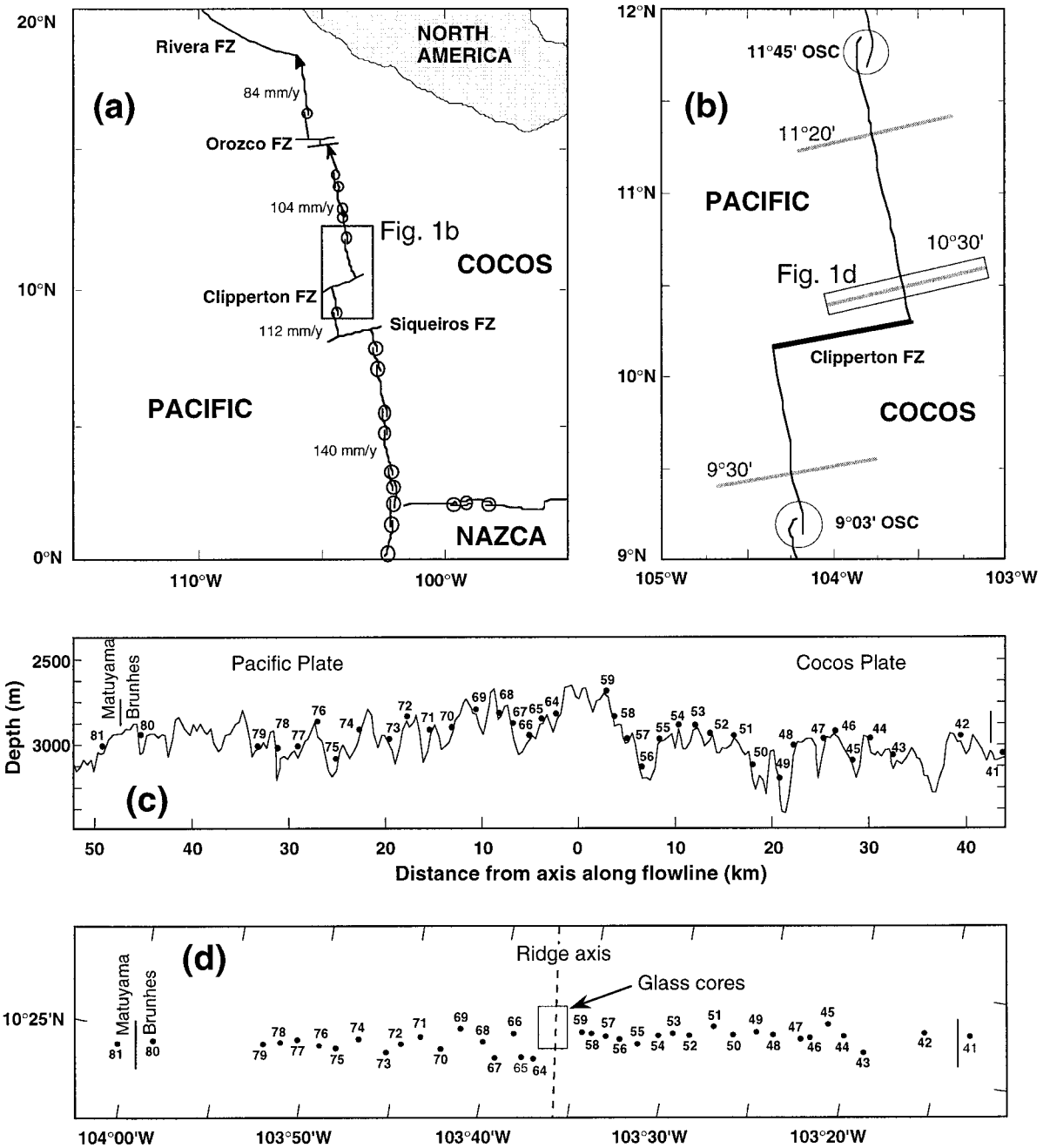

Fig. 1. (a) Simplified tectonic map of the northern EPR, showing location of the studied area. (b) Simplified tectonic map of the EPR between 9° and 12°N, to show the location of the samples dredged from off-axis during the Phoenix 02 expedition. (c) Cross-section through the EPR axis. (d) Detailed map of the EPR at 10°30′N, showing locations of samples collected by dredging and rock coring.

allowed more dense sampling (~2 samples/km^2) of an area of ~12 km^2 within ~3 km of the ridge axis.

This region of the EPR is free of large seamounts, overlapping spreading centers and other complexities in the axial rift system. At 10°30′N, the ridge

axis lies at a depth of ~2800 m, about 200–300 m deeper than much of the EPR axis in this region, and plunges southwards to a depth of over 3000 m at the Clipperton Fracture Zone (CFZ). In contrast to much of the axial system of the northern EPR, the axial rise is poorly developed, and the ridge flanks have a 'rough' topography [21]. Such characteristics may reflect a relatively low magma supply to the ridge axis [27,28]. Much of the EPR between 9º and 14ºN is underlain by a seismic reflecting horizon which has been interpreted as evidence for the presence of magma chambers at a depth of between 1 and 2.5 km beneath the seafloor [1]. In contrast, an axial reflector has not been detected beneath the ridge axis at 10º30′N, although the presence of a crustal low-velocity zone suggests that melt is present, possibly in a mush zone [24]. At 10º30′N, the crustal thickness is essentially normal (~5.5 km [24]), despite the inferred low magma supply. On the other hand, recent studies on the EPR have shown that crustal thickness does not vary in any simple way with magma budget as inferred from ridge axis depth or cross-sectional area [29,30].

The chemistry of MORB from the present-day EPR spreading axis in the 10º30′N region is relatively well known. Thompson et al. [5] analyzed a suite of lavas dredged from between latitudes 10º and 12ºN, and the 10º30′N region was also sampled by Langmuir et al. [8]. Lavas dredged from the ridge axis between 10º20′N and 11º15′N display regular along-axis variations in major and trace element chemistry, although lavas from close to the CFZ have more variable major and trace element compositions [5]. These geochemical gradients led Thompson et al. [5] to suggest that the ridge axis is underlain by a compositionally zoned AMC which extends from the CFZ at its southern end, to the 11º15′N overlapping spreading center (OSC) in the north. The AMC was interpreted to be supplied with melt beneath the shallowest part of the ridge at 11ºN, close to where the hottest, most MgO-rich lavas have been erupted [5].

3. Analytical techniques

Major and trace element data for glasses from 10º30′N are given in Table 1, and Sr, Nd and Pb isotope data in Table 2. Major element analyses were carried out by electron microprobe at LDEO and SOEST, and all data are normalized to a Smithsonian MORB glass reference standard VG-2, whose working values (SiO_2, 50.57 wt%; TiO_2, 1.85%; Al_2O_3, 14.06%; FeO_t, 11.59%; MnO, 0.22%; MgO, 7.07%; CaO, 11.12%; Na_2O, 2.63%; K_2O, 0.19%; P_2O_5, 0.20%) were agreed upon by J. Karsten, E. Klein and Y. Niu in 1993, and which is used as an inter-laboratory standard for MORB glass probe analyses. The major element analyses are available as an **EPSL Online Background Data Set** [1]. Trace element analyses were carried out on a Fisons Plasmaquad II inductively coupled plasma mass spectrometer at The University of Queensland; details of sample preparation and analytical conditions are given elsewhere [31].

All trace element and isotope measurements were carried out on handpicked glass chips. Material with visible Mn oxide coating or alteration products was discarded. Before digestion for trace element and isotope analysis, samples were leached for 10 min at room temperature in H_2O_2–HCl, in order to remove Fe–Mn oxide coatings from the glass. 100–150 mg of glass was dissolved for Sr and Nd isotope analyses, Pb isotope analyses were carried out on a separate dissolution. Sr, Nd and Pb were separated using standard ion-exchange procedures, blanks were below 0.7, 0.4, and 0.2 ng for Sr, Nd and Pb, respectively. All isotope measurements were carried out at The University of Queensland on a VG Sector 54-30 mass spectrometer in static mode. For Sr and Nd analyses, an exponential fractionation correction was applied using $^{86}Sr/^{88}Sr = 0.1194$ and $^{146}Nd/^{144}Nd = 0.7219$. Ten analyses of the NBS 987 Sr standard over the period of analysis yielded $^{87}Sr/^{86}Sr = 0.710267 \pm 15$ (2σ), and five analyses of an Ames metal Nd standard gave $^{143}Nd/^{144}Nd = 0.511969 \pm 9$ (2σ). Data in Table 1 have been normalized to values of 0.710248 and 0.511972 (the value of the Ames Nd standard relative to a value of 0.511855 for the La Jolla standard). Pb isotope measurements were corrected for mass fractionation (typically 1.4‰ per amu) determined from 2 to 3 analyses of the NBS 981 Pb standard during each run.

[1] http://www.elsevier.nl/locate/epsl, mirror site: http://www.elsevier.com/locate/epsl

4. Were the samples erupted at the ridge axis?

Samples collected from off-axis can be used to examine temporal changes in MORB chemistry, provided that flows on the ridge flanks were originally erupted close to the ridge axis, so that their ages may be estimated from the spreading rate. Previous geochemical and geological studies of the EPR have shown that although magmatism generally appears to be limited to within about 2 km of the ridge axis, flows may also be emplaced up to at least 4 km off-axis [32]. Sampling of the topmost flows on the ridge flanks (for example by rock coring) could therefore preferentially sample younger flows emplaced off-axis. However, most of the samples analyzed in this study were dredged from fault scarps which expose 100–200 m of section, rather than the uppermost flows at any dredge location. On the other hand, talus from younger flows, or lavas from syntectonic eruptions, may have covered the fault scarps [33]. An ^{40}Ar–^{39}Ar study of 11 samples from the flanks of the EPR between 9°30′N and 11°20′N found that of 17 analyses, 4 analyses (of 3 different flows) gave ages that were younger (at the 1σ level) than the age predicted from the spreading rate [34]. The average error on the ^{40}Ar–^{39}Ar analyses is 75 ka, suggesting that most of the flows sampled were emplaced within about 4 km of the ridge axis.

The likely effect of sampling flows erupted off-axis will be an increase in the geochemical variation observed at each dredge location. The symmetrical variation in the average major element chemistry of samples erupted on each side of the spreading axis at 10°30′N (Fig. 2) cannot be explained by off-axis magmatism. Samples from both sides of the ridge axis have a similar range in major element chemistry, and lie along broadly similar liquid lines of descent (Fig. 3). In detail, there are differences between the most evolved samples (MgO <4.5%) from each side of the axis, but the range of compositions in Fig. 3b is similar to that seen in the evolved suite of lavas erupted along the East Galapagos Rift [35].

The mean spacing of the dredge samples (~1.6 km) is comparable to the dimensions of individual flows (less than about 1 km [36]), but smaller than the half-width of the neovolcanic zone at the ridge axis (less than about 4 km, as discussed above). The dredge samples can therefore be used to investigate

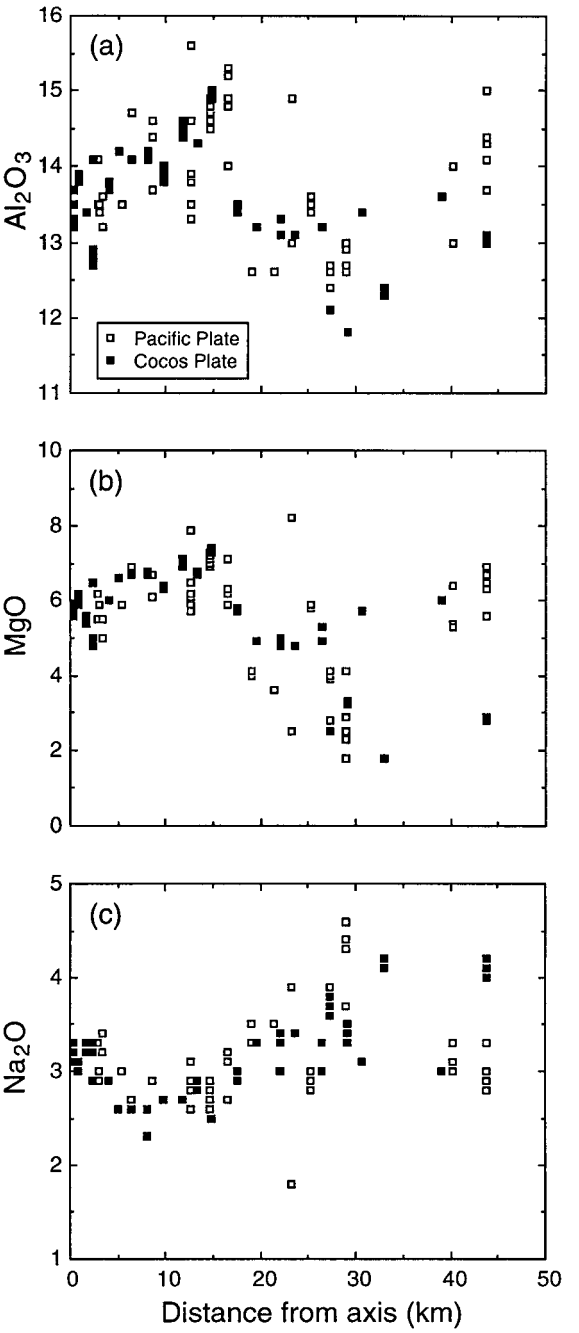

Fig. 2. Variation in (a) Al_2O_3, (b) MgO and (c) Na_2O of the dredged lavas as a function of distance from the present-day ridge axis, measured along a flowline. Open symbols for samples from west of the spreading axis (Pacific Plate), closed symbols for samples from east of the spreading axis (Cocos Plate). Note the broadly symmetrical variation in lava chemistry about the EPR axis.

Table 1
Major and trace element data for lavas from the East Pacific Rise at 10°30′N

Sample	PH44-2	PH45-1	PH46-3	PH47-3	PH49-SG	PH51-5	PH52-2	PH54-3	PH55-3	PH56-2	PH59-2	PH60-2	PH62-1	PH63-1	PH64-2	GC-74
Latitude (°N)	10.526	10.534	10.517	10.519		10.514	10.499	10.499	10.482	10.488	10.490	10.480	10.483	10.477	10.456	10.496
Longitude (°W)	103.340	103.361	103.372	103.383		103.466	103.484	103.510	103.529	103.550	103.583	103.599	103.614	103.617	103.626	103.622
Depth (m)	3153	3169	3066	3192		3154	3053	3069	3170	3178	2874	2831	2812	2832	3008	2913
Age (ka) [a]	617	586	546	531		351	297	238	194	160	81	48	16	9	51	<50
SiO_2	51.41	51.60	54.17	51.37		51.64	51.11	50.95	50.82	50.80	51.04	50.27	50.50	50.73	50.602	50.71
TiO_2	2.24	3.63	2.74	2.59		2.44	1.54	1.77	2.34	2.28	2.62	3.21	2.25	2.57	2.520	2.52
Al_2O_3	13.44	11.79	12.12	13.24		13.42	14.87	14.46	13.98	14.23	13.77	12.91	13.87	13.22	13.45	13.45
FeO	12.93	17.01	15.62	13.31		12.86	9.82	10.84	12.45	11.94	12.56	15.33	12.85	13.75	13.97	13.71
MnO	0.25	0.32	0.30	0.21		0.25	0.18	0.21	0.23	0.22	0.23	0.25	0.24	0.23	0.21	0.25
MgO	5.73	3.27	2.51	5.28		5.66	7.39	6.99	6.31	6.67	6.01	4.94	6.10	5.62	5.51	5.50
CaO	10.05	7.61	6.84	10.27		10.19	11.97	11.56	10.77	11.09	10.50	9.12	10.62	10.06	9.96	10.24
Na_2O	3.13	3.41	3.84	3.01		2.91	2.52	2.69	2.71	2.27	2.90	3.29	3.06	3.30	3.27	3.11
K_2O	0.18	0.38	0.59	0.20		0.19	0.13	0.12	0.16	0.16	0.20	0.26	0.19	0.21	0.22	0.19
P_2O_5	0.21	0.53	0.74	0.23		0.19	0.14	0.13	0.19	0.21	0.24	0.28	0.25	0.20	0.21	0.21
Total	99.57	99.54	99.49	99.72		99.74	99.67	99.73	99.96	99.89	100.06	99.87	99.93	99.88	99.91	99.89
Li	9.25	16.7	21.1	12.3	8.97	8.64	5.61	6.90	8.71	8.12	8.82	8.46	8.19	9.44	8.60	7.89
Be	0.654	1.49	1.99	1.08	1.15	0.642	0.374	0.460	0.598	0.562	0.720	0.644	0.639	0.704	0.683	0.568
Sc	43.4	35.9	30.8	41.3	38.7	42.9	38.9	43.6	42.4	43.2	43.9	44.1	43.5	43.3	44.6	41.4
V	363	232	114	347	293	359	258	308	371	351	375	361	342	386	366	343
Cr	15.6	0.121	0.114	14.1	59.4	29.3	271	161	177	155	133	81.7	82.2	14.0	78.9	85.2
Co	47.6	38.3	29.6	43.8	40.3	45.7	41.5	45.8	45.1	45.6	45.0	45.9	45.0	47.9	46.0	43.4
Ni	32.0	4.52	2.61	27.2	37.6	36.9	81.0	64.4	64.3	66.0	55.3	72.7	71.9	31.6	52.6	43.7
Cu	75.5	53.8	42.9	70.8	68.1	71.4	72.8	86.9	69.2	72.6	75.6	74.3	74.8	77.2	74.2	70.9
Zn	117	178	195	141	124	118	76.8	92.4	117	105	128	115	119	123	114	97.1
Ga	19.6	24.4	26.5	21.7	22.1	19.4	15.2	17.5	19.2	18.2	19.5	19.0	19.0	20.1	19.1	18.5
Rb	2.47	5.09	7.83	3.77	3.52	1.82	1.24	1.23	2.01	2.01	2.37	1.99	2.01	2.22	1.97	2.07
Sr	125	120	128	127	119	120	104	111	102	110	120	128	131	126	128	127
Y	44.4	94.5	117	63.1	76.9	43.0	26.3	33.3	43.2	40.5	46.3	42.7	40.2	47.1	43.21	37.7
Zr	143	348	463	236	284	137	76.8	98.7	131	127	154	143	133	156	145	128
Nb	4.45	12.6	16.9	8.50	9.17	4.69	2.78	2.68	4.53	4.57	5.39	4.78	4.61	5.23	4.83	4.49
Cs	0.088	0.076	0.117	0.059	0.050	0.031	0.024	0.024	0.032	0.032	0.038	0.031	0.035	0.034	0.031	0.029
Ba	17.6	42.1	64.0	33.5	28.2	17.4	11.8	9.82	17.6	18.0	21.1	18.5	19.2	20.5	18.7	19.7
La	5.47	13.9	19.3	9.35	10.8	5.27	3.06	3.51	5.00	4.95	6.00	5.47	5.25	5.98	5.58	5.03
Ce	17.0	42.1	57.7	28.0	33.5	16.6	9.51	11.6	15.7	15.4	18.5	17.2	16.3	18.7	17.4	15.4
Pr	3.05	7.34	9.90	4.87	5.94	2.95	1.72	2.12	2.85	2.75	3.31	3.08	2.90	3.31	3.07	2.63
Nd	15.1	35.9	47.7	23.4	28.7	14.5	8.44	10.6	14.1	13.6	16.2	14.9	4.2	16.5	15.1	13.5
Sm	5.12	11.4	14.7	7.43	9.04	4.81	2.88	3.68	4.75	4.59	5.33	4.88	4.64	5.35	4.99	4.60
Eu	1.75	3.51	4.26	2.25	2.78	1.69	1.07	1.32	1.67	1.58	1.80	1.72	1.66	1.92	1.74	1.60
Gd	6.92	15.2	18.9	9.66	12.0	6.55	3.92	5.06	6.56	6.25	7.13	6.57	6.25	7.27	6.70	1.05
Tb	1.15	2.53	3.15	1.65	2.03	1.13	0.682	0.868	1.12	1.06	1.21	1.12	1.06	1.25	1.14	6.01
Dy	7.85	17.0	20.8	11.1	13.6	7.64	4.68	5.93	7.58	7.19	8.07	7.47	7.08	8.35	7.69	7.08
Ho	1.67	3.61	4.45	2.37	2.91	1.65	0.993	1.26	1.64	1.55	1.77	1.63	1.54	1.82	1.66	1.52
Er	4.91	10.6	12.9	6.91	8.48	4.85	2.93	3.74	4.85	4.53	5.08	4.73	4.49	5.29	4.82	4.34
Tm	0.695	1.50	1.84	0.994	1.21	0.681	0.409	0.517	0.673	0.638	0.708	0.666	0.635	0.752	0.678	0.647
Yb	4.57	9.85	12.0	6.55	8.07	4.57	2.73	3.51	4.48	4.24	4.73	4.41	4.17	4.95	4.50	4.12
Lu	0.685	1.48	1.80	0.989	1.21	0.692	0.409	0.524	0.524	0.679	0.714	0.641	0.615	0.737	0.672	0.629
Hf	3.88	9.43	12.0	6.19	7.62	3.76	2.10	2.73	3.61	3.44	4.04	3.75	3.58	4.22	3.87	3.59
Ta	0.294	0.845	1.07	0.541	0.606	0.328	0.185	0.441	0.295	0.302	0.357	0.317	0.307	0.355	0.324	0.304
Pb	0.554	1.20	1.65	0.805	0.608	0.563	0.314	0.374	0.499	0.498	1.00	0.872	0.654	0.715	0.588	0.535
Th	0.252	0.738	1.04	0.545	0.577	0.268	0.152	0.150	0.267	0.252	0.305	0.272	0.257	0.297	0.267	0.258
U	0.109	0.296	0.413	0.219	0.226	0.108	0.060	0.061	0.103	0.105	0.123	0.117	0.135	0.119	0.114	0.103

Table 1 (continued)

Sample	PH65-1	PH64-3	PH66-2	PH68-1	PH69-2	PH70-2	PH72-3	PH76-3	PH77-6	PH78-1	PH78-2	PH78-5	PH79-1	PH79-2	GC-78	GC-83
Latitude (°N)	10.453	10.456	10.474	10.463	10.473	10.473	10.445	10.428	10.432	10.427	10.427	10.427	10.422	10.422	10.500	10.490
Longitude (°W)	103.635	103.626	103.624	103.675	103.701	103.701	103.752	103.824	103.850	103.859	103.859	103.859	103.883	103.883	103.604	103.620
Depth (m)	2996	3008	3075	2947	3007	3007	3078	3228	3051	3058	3058	3058	3097	3097	2872	2916
Age (ka) [a]	60	51	56	114	153	153	261	412	450	484	484	484	516	516	<50	<50
SiO_2	50.790	50.613		50.434	50.574	50.538	50.23	53.46	51.53	55.85	52.72	53.29	57.95	52.11	51.13	50.93
TiO_2	2.512	2.369		2.071	1.931	2.204	1.63	2.63	2.55	2.56	3.20	2.78	2.07	2.91	2.27	2.55
Al_2O_3	13.602	14.074		14.650	14.426	13.749	14.81	12.96	13.49	12.56	12.42	12.42	12.93	12.58	13.78	13.51
FeO	13.57	12.53		11.10	11.31	12.91	10.90	15.73	12.39	14.08	14.74	14.11	11.80	14.92	12.65	13.13
MnO	0.24	0.24		0.20	0.22	0.25	0.21	0.32	0.25	0.25	0.26	0.25	0.22	0.25	0.22	0.25
MgO	5.53	6.20		6.87	6.73	6.10	7.25	2.49	5.84	2.83	3.90	4.11	2.90	4.07	5.79	5.62
CaO	10.11	10.57		11.41	11.45	10.85	11.68	7.04	10.32	6.84	7.99	8.20	6.49	8.44	10.74	10.24
Na_2O	3.16	2.93		2.71	2.91	2.90	2.87	3.85	2.98	3.89	3.68	3.71	4.29	3.73	2.83	3.20
K_2O	0.19	0.19		0.19	0.17	0.16	0.17	0.64	0.19	0.53	0.38	0.37	0.76	0.38	0.19	0.20
P_2O_5	0.25	0.21		0.25	0.17	0.25	0.16	0.75	0.23	0.52	0.48	0.47	0.34	0.49	0.20	0.22
Total	99.94	99.93		99.87	99.88	99.91	99.91	99.86	99.76	99.90	99.76	99.71	99.76	99.88	99.79	99.86
Li	10.6	11.0	9.98	7.56	7.04	8.30	6.71	16.8	9.38	16.2	13.1	12.6	22.9	17.8	9.16	8.95
Be	0.784	0.900	0.728	0.623	0.489	0.550	0.525	1.74	0.690	1.74	1.39	1.35	2.30	1.91	0.647	0.687
Sc	51.6	43.4	42.8	44.5	42.2	44.8	43.7	32.4	43.0	28.9	37.0	35.6	26.6	31.6	41.0	41.2
V	454	455	409	342	302	370	292	221	392	174	274	261	176	210	385	382
Cr	43.5	4.36	161	229	120	107	236	3.88	26.3	1.75	18.2	16.6	6.00	12.2	23.4	34.4
Co	57.1	49.5	46.9	45.3	45.9	49.3	44.9	34.5	46.6	29.3	39.4	37.5	26.8	32.8	46.3	45.8
Ni	47.2	29.7	71.9	71.0	60.0	52.6	70.0	11.8	34.4	6.52	18.2	17.1	10.6	13.6	33.5	41.4
Cu	91.9	77.4	65.6	83.7	77.2	86.0	81.5	56.1	74.9	45.6	65.1	62.0	45.9	55.0	74.9	73.9
Zn	143	140	132	96.7	91.1	108	90.4	167	126	157	166	143	131	144	115	113
Ga	23.1	21.1	20.2	18.0	17.4	18.7	17.3	24.9	19.7	25.1	23.3	22.6	25.2	24.8	20.0	19.8
Rb	2.41	2.55	2.25	2.34	1.54	1.82	1.52	6.35	2.21	6.95	4.75	4.64	11.0	7.54	2.03	2.17
Sr	148	132	112	134	120	104	126	128	117	121	121	118	110	117	126	133
Y	54.2	57.1	51.9	39.7	33.1	42.1	31.5	99.6	47.8	107	84.0	83.1	111	103	44.2	43.9
Zr	176	203	163	135	104	127	102	408	154	426	317	315	498	443	151	155
Nb	5.77	6.58	5.68	4.89	3.83	3.72	4.05	13.42	5.03	14.4	11.1	10.8	17.7	15.1	4.77	5.13
Cs	0.033	0.036	0.034	0.034	0.023	0.026	0.022	0.082	0.035	0.086	0.066	0.062	0.143	0.096	0.027	0.029
Ba	21.7	23.1	20.9	20.4	15.4	13.7	15.8	49.7	18.6	51.4	38.2	36.9	80.2	58.2	19.2	20.7
La	6.72	7.80	6.18	5.46	4.20	4.59	4.28	15.69	5.70	16.91	12.6	12.3	21.2	17.5	5.61	5.86
Ce	21.2	24.3	19.6	16.8	12.8	14.9	12.8	47.6	18.0	50.2	37.9	37.4	61.0	51.7	17.6	18.2
Pr	3.78	4.26	3.54	2.93	2.27	2.71	2.22	8.24	3.24	8.82	6.60	6.44	9.96	8.69	3.04	3.12
Nd	19.0	20.8	17.8	14.3	11.2	13.7	10.9	39.3	16.1	42.0	32.1	31.2	45.1	40.7	15.8	16.0
Sm	6.21	6.66	5.97	4.64	3.68	4.68	3.57	12.2	5.36	13.2	10.2	10.1	13.7	12.7	5.38	5.41
Eu	2.21	2.31	2.12	1.64	1.34	1.65	1.30	3.52	1.86	3.73	3.05	2.99	3.42	3.41	1.85	1.87
Gd	8.40	9.03	8.21	6.32	5.11	6.40	4.86	15.8	7.25	17.4	13.3	13.1	17.0	16.1	1.23	1.22
Tb	1.43	1.51	1.37	1.06	0.863	1.09	0.817	2.64	1.26	2.83	2.24	2.22	2.89	2.69	6.95	6.98
Dy	9.69	10.3	9.29	7.07	5.87	7.44	5.60	17.6	8.41	18.9	15.1	14.8	19.4	18.0	8.27	8.17
Ho	2.09	2.20	2.02	1.52	1.28	1.60	1.21	3.82	1.83	4.04	3.24	3.18	4.20	3.90	1.77	1.75
Er	6.04	6.45	5.84	4.47	3.69	4.70	3.56	11.2	5.33	11.8	9.52	9.37	12.7	11.6	5.06	4.99
Tm	0.851	0.907	0.825	0.629	0.525	0.663	0.506	1.60	0.744	1.71	1.33	1.32	1.79	1.64	0.754	0.746
Yb	5.71	5.98	5.45	4.15	3.44	4.40	3.28	10.4	4.96	11.2	8.82	8.73	12.0	11.0	4.83	4.75
Lu	0.845	0.888	0.805	0.617	0.517	0.640	0.487	1.57	0.749	1.67	1.33	1.33	1.80	1.66	0.735	0.723
Hf	4.88	5.41	4.54	3.62	2.82	3.55	2.69	10.6	4.21	11.2	8.48	8.36	13.2	11.6	4.18	4.22
Ta	0.390	0.438	0.387	0.322	0.257	0.246	0.261	0.864	0.338	0.902	0.718	0.701	1.12	0.975	0.323	0.344
Pb	0.726	0.790	0.599	0.523	0.422	0.449	0.451	1.31	0.572	1.40	0.978	0.944	1.977	1.418	0.608	0.629
Th	0.315	0.368	0.290	0.270	0.221	0.211	0.220	0.883	0.280	1.04	0.693	0.681	1.572	1.138	0.272	0.289
U	0.134	0.158	0.123	0.113	0.090	0.090	0.096	0.362	0.115	0.393	0.277	0.281	0.625	0.456	0.109	0.117

Major element concentrations in wt%, trace element concentrations in ppm. Analytical procedures are described in detail in the text. Samples with GC- prefix were collected by rock coring.

[a] Approximate age of each sample was calculated using the half-spreading rates determined for this ridge segment by Carbotte and Macdonald [16].

Table 2
Isotope data for samples from 10°30′N

Sample	$^{87}Sr/^{86}Sr$	$^{143}Nd/^{144}Nd$	$^{206}Pb/^{204}Pb$	$^{207}Pb/^{204}Pb$	$^{208}Pb/^{204}Pb$
PH44-2	0.702679 ± 9	0.513157 ± 7	18.315	15.484	37.738
PH45-1	0.702537 ± 9	0.513159 ± 6	18.299	15.480	37.718
PH46-3	0.702542 ± 9	0.513148 ± 7	18.285	15.478	37.693
PH47-3	0.702559 ± 9	0.513152 ± 7	18.337	15.494	37.769
49SG	0.702618 ± 9	0.513161 ± 7	18.315	15.490	37.763
PH51-2			18.388	15.531	37.856
PH51-5	0.702519 ± 9	0.513167 ± 7	18.311	15.479	37.723
PH52-2	0.702538 ± 9	0.513150 ± 7			
PH54-3	0.702470 ± 9	0.513180 ± 7	18.248	15.463	37.607
PH55-3	0.702527 ± 9	0.513153 ± 7	18.321	15.467	37.706
PH56-2	0.702549 ± 9	0.513159 ± 7	18.322	15.492	37.758
PH59-2	0.702548 ± 9	0.513145 ± 6	18.322	15.488	37.749
PH60-2	0.702534 ± 9	0.513157 ± 6	18.296	15.475	37.703
PH62-1	0.702540 ± 9	0.513150 ± 6	18.321	15.497	37.762
PH63-1	0.702546 ± 9		18.347	15.492	37.779
PH64-2	0.702536 ± 9	0.513140 ± 6	18.270	15.460	37.663
PH65-1	0.702531 ± 9	0.513162 ± 7	18.303	15.484	37.724
PH64-3	0.702530 ± 9	0.513162 ± 7			
PH66-2	0.702545 ± 9	0.513163 ± 7	18.296	15.464	37.663
PH68-1	0.702592 ± 9	0.513167 ± 6	18.307	15.492	37.732
PH69-2	0.702552 ± 9	0.513156 ± 7	18.338	15.484	37.754
PH70-2	0.702531 ± 9	0.513159 ± 7			
PH72-3	0.702519 ± 9	0.513162 ± 7			
PH76-3	0.702530 ± 9	0.513161 ± 7	18.291	15.469	37.682
PH77-6	0.702508 ± 9	0.513173 ± 6	18.305	15.490	37.737
PH78-1	0.702568 ± 9	0.513166 ± 7	18.293	15.477	37.692
PH78-2	0.702549 ± 9	0.513155 ± 8	18.288	15.472	37.675
PH78-5	0.702566 ± 9	0.513172 ± 7	18.290	15.471	37.675
PH79-1	0.702592 ± 9	0.513157 ± 7	18.313	15.480	37.720
PH79-2	0.702583 ± 9	0.513151 ± 7	18.304	15.478	37.707
GC-74	0.702559 ± 9	0.513140 ± 7			
GC-78		0.513142 ± 6			
GC-83	0.702566 ± 10	0.513155 ± 7			

Errors are 2σ and refer to the final digits. Analytical procedures are described in detail in the text.

changes in the composition of the lavas that were erupted at the ridge axis over periods of 200–300 ka. The ages of the samples used in Fig. 4 and in the following discussion were calculated using the half-spreading rates for this ridge segment determined from magnetic studies [16].

5. Results

5.1. General geochemistry of lavas from 10°30′N

Lavas from the 10°30′N region span a very wide compositional range, and include basalts, basaltic andesites and andesites (Fig. 3). The most evolved lavas (1–4% MgO) were recovered in dredges from 400–800 ka old seafloor, on both the eastern and western flanks of the ridge axis (Fig. 4). Elsewhere on the EPR, highly evolved lavas such as these are rare, and are most often found close to discontinuities in the axial ridge system, for example propagating rifts [35,37], major transform faults or overlapping spreading centers [8,38]. However, highly evolved lavas appear to be common on the seafloor immediately north of the CFZ. Samples with <5% MgO have been dredged from the present-day ridge axis between 10°17′ and 10°21′N [5,8], and highly evolved lavas have been recovered in dredges from

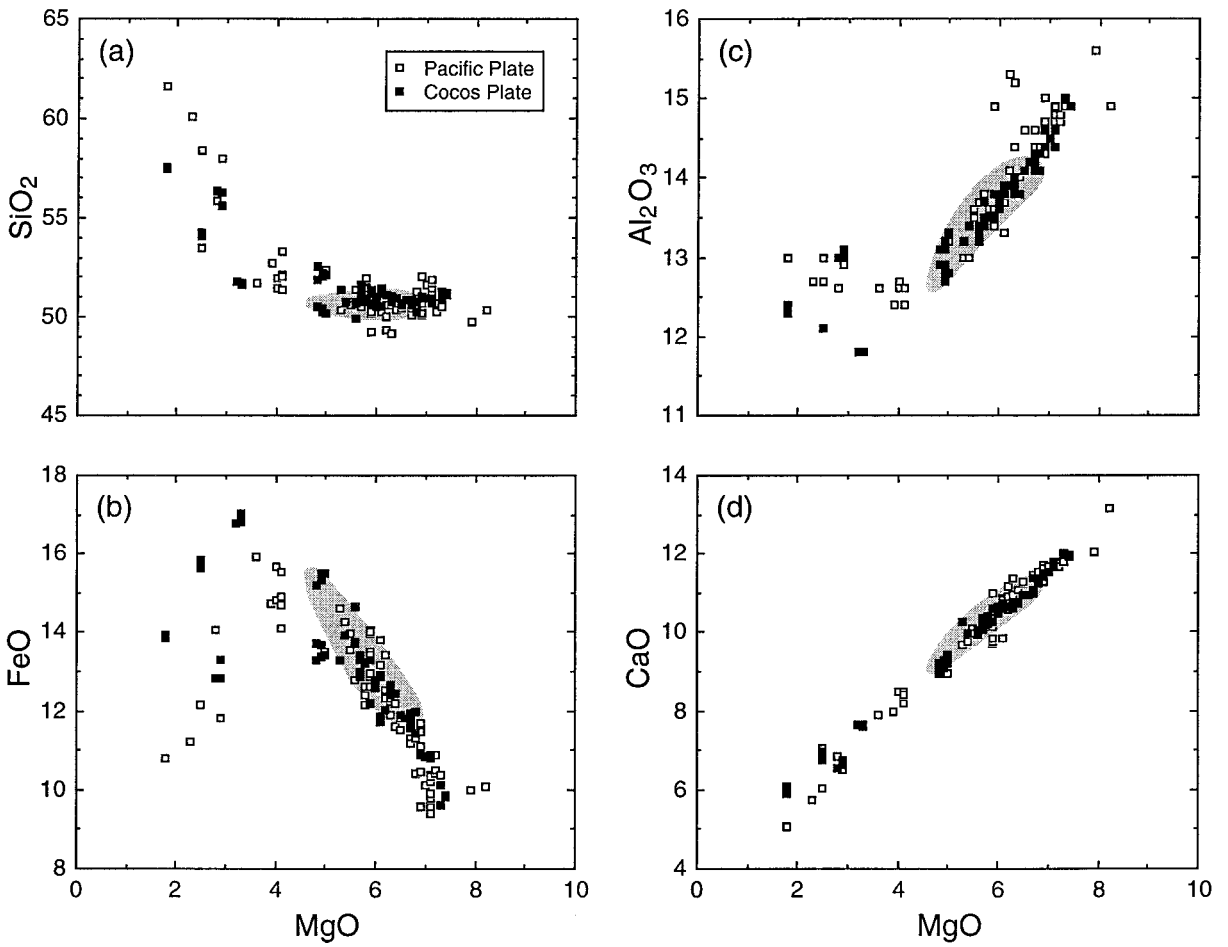

Fig. 3. Variation in (a) SiO_2, (b) FeO, (c) Al_2O_3, and (d) CaO with MgO for samples dredged from 10°30′N. Field for core samples (younger than about 50 ka) is also shown. Samples from each side of the ridge axis display a similar range in major element chemistry.

seafloor up to 1.4 Ma old north of the CFZ [39,40]. The presence of evolved lavas on the seafloor to the north of the CFZ has also been inferred from magnetic data [16]. In contrast, such evolved rocks have not been found on the magmatically robust axis to the south of the CFZ, nor have they been recovered in dredges on older seafloor on the southern side of the CFZ [9,39].

Lavas from 10°30′N display large variations in trace element concentrations, consistent with large extents of fractional crystallization (Fig. 5a,b). However, incompatible trace element ratios indicate that not all of the lavas (e.g. samples 54-3, 70-2; Fig. 5e) can be related by fractional crystallization. The andesites and basaltic andesites have $[La/Sm]_N$ and K_2O/TiO_2 ratios of up to 1.0 and 0.6, respectively, as a result of fractional crystallization, but all samples with MgO >5% have $[La/Sm]_N$ <0.9 and K_2O/TiO_2 <0.15 (Fig. 5) and are thus NMORB. No EMORB were recovered at 10°30′N, nor have any been dredged from the axis along this segment of the EPR [5,8,40].

All samples have Sr, Nd and Pb isotope compositions that are typical of Pacific MORB. Excluding samples 54-3 and 44-2, $^{87}Sr/^{86}Sr$ varies between 0.70251 and 0.70259 (Fig. 5). Sr and Nd isotope data for three of the rock core samples lie within the range of the older samples dredged from the ridge flanks. The 10°30′N lavas have slightly higher $^{87}Sr/^{86}Sr$ than lavas from the ridge segment immediately to

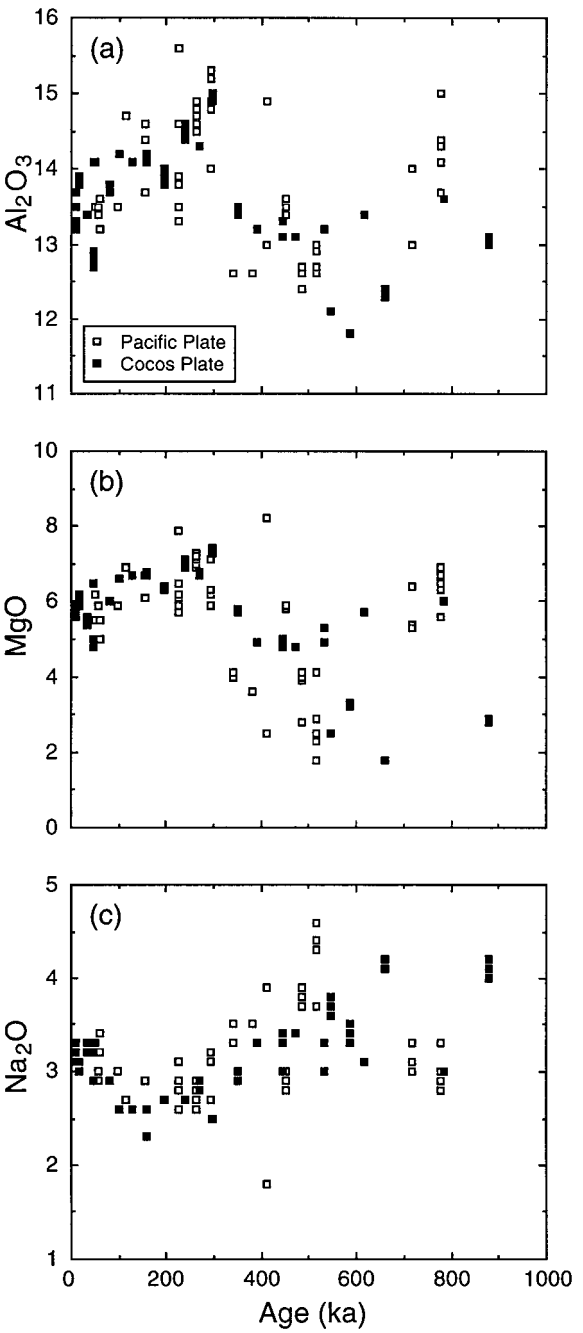

Fig. 4. Variation in (a) Al_2O_3, (b) MgO and (c) Na_2O of glasses dredged from 10°30′N with theoretical eruption age, calculated assuming half spreading rates of 4.982 cm/yr (east) and 5.618 cm/yr (west) for the period 0–730 ka, and 7.412 cm/yr (east) and 6.188 cm/yr (west) for the period 730–950 ka [16].

the south of the CFZ at 9°30′N, most of which have values in the range 0.70248–0.70252 [6,41].

5.2. Temporal chemical variations

As discussed in Section 4, we believe that most of the lavas at 10°30′N were emplaced within about 4 km of the ridge axis, allowing the age of the dredge samples to be estimated from the spreading rate, to within about 75 ka. The samples can thus provide information on changes in the compositions of the lavas erupted at the ridge axis, over periods of 200–300 ka.

During the past 800 ka, there have been significant variations in the major element chemistry of the lavas erupted on this segment of the EPR (Fig. 4). The temporal variations in major element chemistry are most clearly seen when the average of three adjacent dredges (equivalent to a period of about 90 ka, which is similar to the estimated uncertainty in the calculated age of each sample) is considered (Fig. 6). For example, the average MgO content of lavas erupted on both sides of the ridge axis increased from about 3.0% at 600 ka, to about 7.0% at 300 ka. Since 300 ka the average MgO has decreased, and the average MgO content of samples collected from within the neovolcanic zone (younger than 50 ka) is 6.0%. The origin of the temporal variations in the average major element chemistry of lavas recorded by the dredge samples is discussed in Section 6.1.

Large variations in trace element abundances in lavas during the past 800 ka (Fig. 5) mirror the variations in major element chemistry, and are related to the degree of fractionation. There have also been significant variations in Sr, Nd and Pb isotope ratios, and in the ratios of highly incompatible trace elements over the past 800 ka, but these variations are not systematic and do not mirror the changes in major element chemistry (Fig. 5).

The 30 rock core samples collected from close to the ridge axis record chemical variations on a much finer scale than the dredged samples. On this length scale, the patterns of chemical variation observed in lavas may reflect the size and shape of individual lava flows, the width of the neovolcanic zone, and the effects of off-axis magmatism, as well as temporal changes in the chemistry of lavas [17,20]. Most of these parameters are very poorly known, and may

vary with spreading rate and the magmatic budget of the ridge axis. All of the core samples were collected from within 3 km of the ridge axis, and are thus younger than 50 ka. The variation in major element chemistry of the core samples is significantly less than the total variation seen in the dredge samples (Fig. 3).

5.3. Comparison with results of previous studies

Most previous geochemical studies of older lavas collected from the flanks of the EPR have been restricted to samples from the seafloor within about 10 km of the ridge axis (less than about 200 ka old). Differences in sampling technique, and sampling density also need to be taken into account when geochemical variations between suites of lavas from different areas are compared.

Previous studies have documented variations both in the major element chemistry of NMORB lavas, and in the relative proportions of NMORB and EMORB, on the scale of a few kilometers on the flanks of the northern EPR and Juan de Fuca Ridge [15,17–19,23]. These chemical variations were interpreted to reflect temporal changes in the chemistry of magma erupted over periods of 50–200 ka. It is not yet clear whether these chemical variations occur in response to magmatic 'cycles' within each ridge segment [15,22]. The degree of chemical variation observed in a given area of seafloor is not the same at every point on the EPR. For example at 12°15′N the major element variation within NMORB samples is smaller than that within NMORB from a comparable area of the seafloor at 9°31′N and at 10°30′N.

Recent high-precision sampling studies using the coring method have shown that chemical heterogeneity of the seafloor exists on very small length scales (less than about 200 m [17,20]). At 9°31′N, at least some of this heterogeneity reflects off-axis emplacement of lavas on the ridge flanks up to about 4 km from the ridge axis [20,32]. On the other hand, a range of up to 2% MgO has been observed in a single dredge haul at many places on the ridge axis, and NMORB and EMORB occur together at many places on the EPR [8,11,17]. Recent multidisciplinary studies of the CoAxial segment of the Juan de Fuca Ridge, have shown that there can be significant chemical variations between flows erupted within 12 years of each other [42]. Thus, on the scale of a few kilometers, the chemical heterogeneity of the seafloor appears to reflect variations in the chemistry of lavas erupted at the axis and throughout the neovolcanic zone on short timescales.

The 10°30′N region differs from most other well-studied regions of the EPR in the absence of EMORB, and in the large variations in major element chemistry of lavas dredged from the ridge flanks, which are far greater than those observed in lavas of similar age span at 9°30′N and 11°20′N [21]. The scarcity of lavas with <4% MgO on the present-day EPR axis suggests that temporal chemical variations as large as those at 10°30′N are not typical of the EPR. On the other hand, the degree of chemical variation observed in the samples cored from within the neovolcanic zone at 10°30′N is very similar to that reported from a similar area of the seafloor at 9°31′N [20].

6. Discussion

6.1. Origin of temporal chemical variations

The systematic variations in the average major element composition of lavas erupted at the ridge axis over the past 800 ka primarily reflect changes in the average degree of fractionation, which is controlled mainly by the rate of melt supply to the ridge axis, relative to the cooling rate [37,43]. Thus, on the EPR, highly differentiated lavas are generally erupted close to large discontinuities in the axial ridge system, where the cooling rate is relatively high, and the melt supply rate may be relatively low. The abundance of highly evolved lavas on the 10°30′N ridge segment could therefore partly reflect the cooling effect associated with the large transform offset which places old, cool crust against the ridge axis at the CFZ. However, this cannot be the only controlling factor, as similarly evolved samples do not occur on the EPR axis immediately south of the CFZ [6,8,39]. This suggests that the melt supply rate is the most important factor in the generation of highly evolved lavas on this ridge segment. Correlations between average MgO content of lavas, and the morphology of the southern EPR ridge axis, also indicate that variations in magma supply rate on time

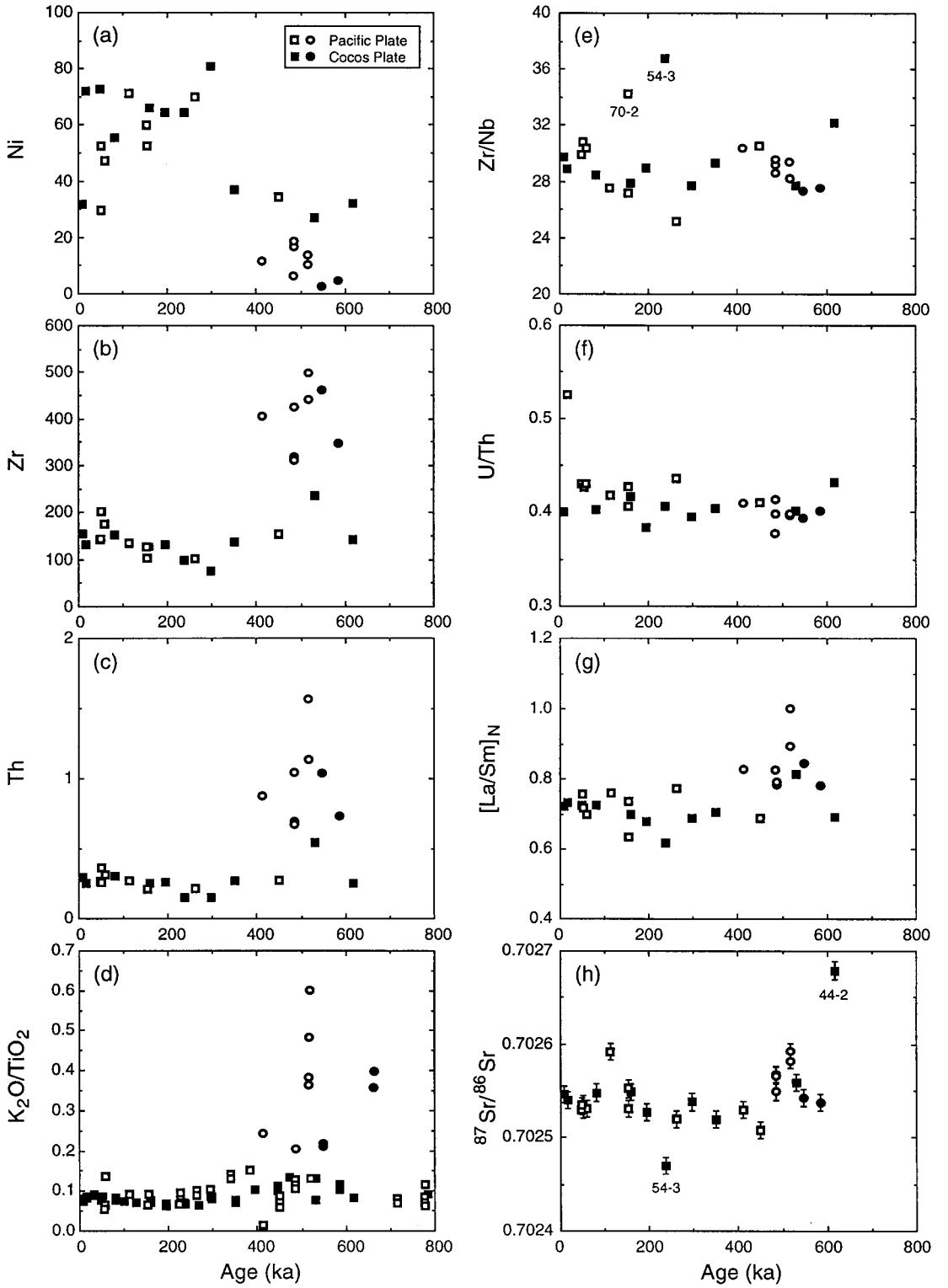
(a)
Pacific Plate
Cocos Plate
Ni
(b)
Zr
(c)
Th
(d)
K2O/TiO2
Age (ka)
(e)
54-3
70-2
Zr/Nb
(f)
U/Th
(g)
[La/Sm]N
(h)
44-2
54-3
87Sr/86Sr
Age (ka)

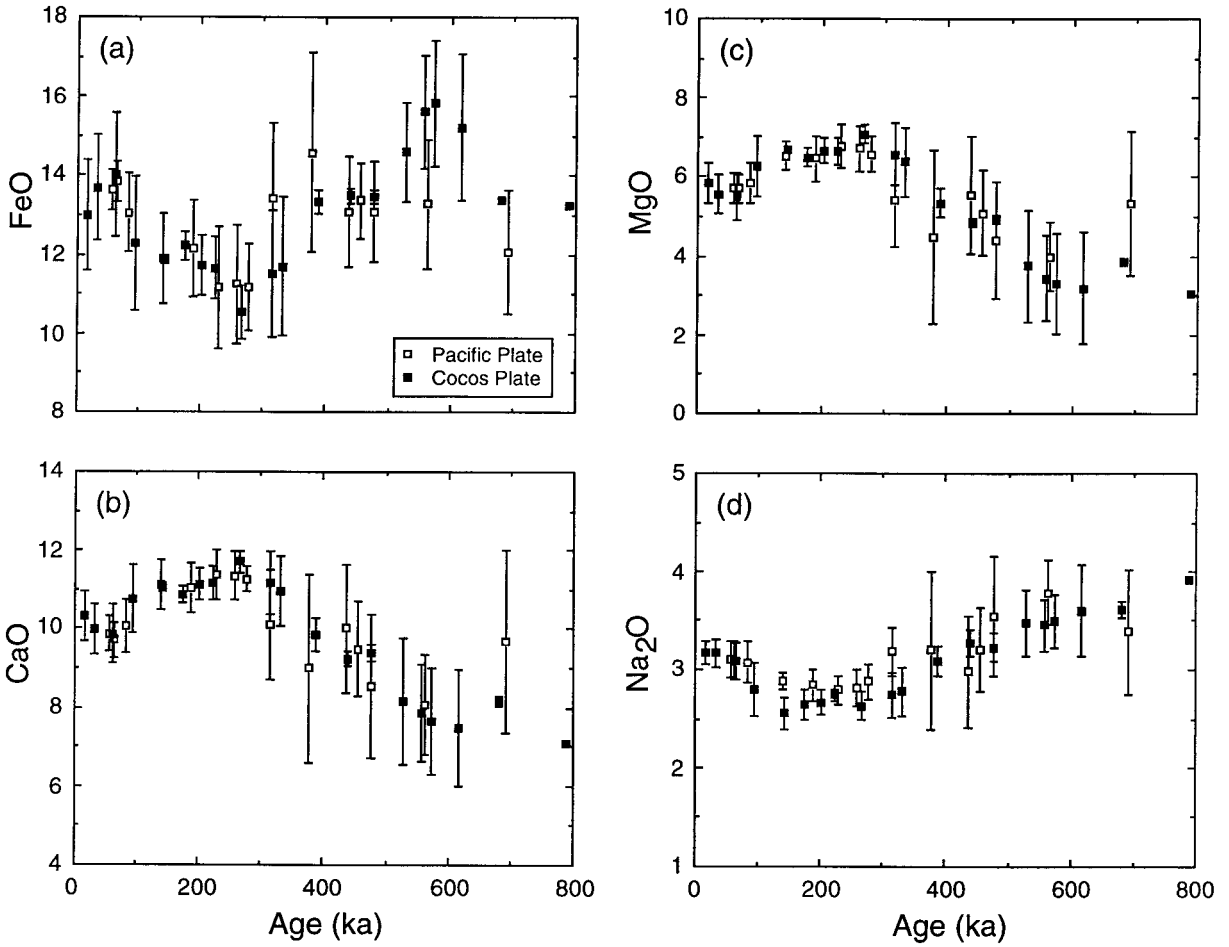

Fig. 6. Variation of (a) FeO, (b) CaO, (c) MgO, and (d) Na_2O with age, calculated from the mean of three adjacent dredge sites, corresponding to a time interval of about 90 ka (the estimated maximum uncertainty in the calculated age of each sample). Error bars represent standard deviation, over a period of 90 ka in order to give an indication of the degree of chemical variability. The smoothed data clearly show the symmetrical chemical variation on each side of the ridge axis, which suggests that most flows were emplaced within about 4 km from the ridge axis.

scales longer than about 100 ka have an important influence on the degree of fractionation of lavas erupted at the axis on the scale of individual ridge segments [29,44]. At 10°30′N, the magma-starved morphology of the ridge axis, and the absence of an AMC seismic reflector suggests that the present rate at which melt is supplied to the ridge axis at 10°30′N is relatively low compared to elsewhere on the EPR [1,27,28].

Further evidence that variations in magma supply rate may occur on timescales on the order of 100 ka has come from studies of the tectonic segmentation of the ridge axis, changes in which may occur in response to variations in the melt supply rate. For

Fig. 5. Variation in (a) Ni, (b) Zr, (c) Th, (d) K_2O/TiO_2, (e) Zr/Nb, (f) U/Th, (g) $[La/Sm]_N$, and (h) $^{87}Sr/^{86}Sr$ with age for lavas dredged from off-axis at 10°30′N. Circular symbols indicate samples with <5% MgO. Temporal variations in incompatible trace element ratios and isotope compositions do not mirror the changes in major element chemistry. Note that all samples with >5% MgO have K_2O/TiO_2 and $[La/Sm]_N$ values typical of NMORB (<0.15 and <1.0, respectively).

example, ridge tip abandonment events at OSCs may occur in response to magmatic cycles in the adjoining ridge segments [45], and a recurrence interval of 50–100 ka has been estimated for the 9°03′N OSC [16]. A similar interval was estimated from the spacing of abandoned ridge tips associated with the 11°45′N OSC [46]. Structures along the northern boundary of the Siqueiros Fracture Zone have been interpreted to reflect a 300–500 ka episodicity in the volcanic and tectonic processes in this region [47].

At 10°30′N, the abundance of relatively evolved lavas on the ridge flanks indicates that the magma supply rate to this ridge segment has been low for much of the past ~800 ka. This is supported by magnetic studies, which suggest that relatively evolved, Fe- and Ti-rich lavas were erupted to the north of the CFZ with a frequency of about 150–350 ka over the past 2 Ma [16]. Although there have been very few geochemical studies of lavas collected from further than 10 km from the ridge axis, chemical variations as great as those seen at 10°30′N are not observed at 9°30 or 11°20 on the EPR [21]. The scarcity of lavas with <5% MgO along the present-day EPR axis suggests that temporal chemical variations as great as those seen at 10°30′N are not typical of the EPR.

As discussed earlier, there have also been significant variations in the major element chemistry of lavas erupted within the last 50 ka inside the neovolcanic zone (Fig. 3). However, without constraints on the age of individual samples, the rate of chemical changes over this period is unknown. Possible mechanisms that could account for chemical variations on timescales of <50 ka are discussed in Section 6.3.

6.2. Comparison of across-axis and along-axis chemical variations

Geochemical studies of lavas dredged from close to the axis on this ridge segment have shown that the compositions of these rocks varies with latitude and axial depth [5,8]. The more Mg-rich lavas were erupted close to the shallowest part of the ridge segment near 11°N, and lavas from further south on the ridge axis, towards the CFZ, are progressively more evolved [5,8] (Fig. 7). Lavas dredged from close to the CFZ have a wide range in compositions. There are also systematic along-axis variations in trace element chemistry (Fig. 7c,d). Thompson et al. [5] argued that the along-axis chemical variations are evidence for the existence of a chemically and thermally zoned magma chamber beneath the ridge axis between 10°20′N and 11°10′N. This magma chamber is inferred to be supplied with magma beneath the axial high at 11°N close to where the most Mg-rich lavas occur, and cooling and crystallization during along-axis transport of melt at crustal levels is responsible for the latitudinal chemical variations.

Lavas dredged from the flanks of the EPR at 10°30′N have a similar range in both major and trace element chemistry to younger lavas recovered from close to the ridge axis along the length of this ridge segment (Fig. 7). At 10°30′N, the chemical variation in samples younger than 50 ka is less than the total variation observed in young lavas from the ridge axis between 10°20′N and 11°10′N, and the average major and trace element composition of the <50 ka lavas from 10°30′N is intermediate between the average compositions of samples from 10°20′N and 10°40′N analyzed by Thompson et al. [5] (Fig. 7). Our new data therefore support the existence of systematic along-axis variations in the chemistry of young lavas erupted at the axis on this ridge segment.

6.3. Model of magma chamber structure at 10°30′N

Our preferred model for the structure of the magma plumbing system beneath the EPR at 10°30′N can account for chemical variability in lavas on a range of timescales, and is broadly similar to models proposed previously for the 9°31′N area [6,20].

Recent geophysical studies have provided some constraints on the shape and size of the axial magma chamber system beneath the EPR. These studies indicate that much of the ridge axis is underlain by a magma chamber which is less than about 2 km wide, and a few hundreds of meters in height, overlying a broader zone of the lower crust containing a few percent of partial melt (e.g. [4]). Early seismic studies did not detect a magma reflector beneath the EPR at 10°30′N [1], although recent seismic profiling of the eastern ridge-transform intersection has revealed the presence of a low-velocity zone consistent with the presence of partial melt, possibly as a magma lens that is too small to be resolved seismically [24]. Thompson et al. [5] argue that focussed melt supply,

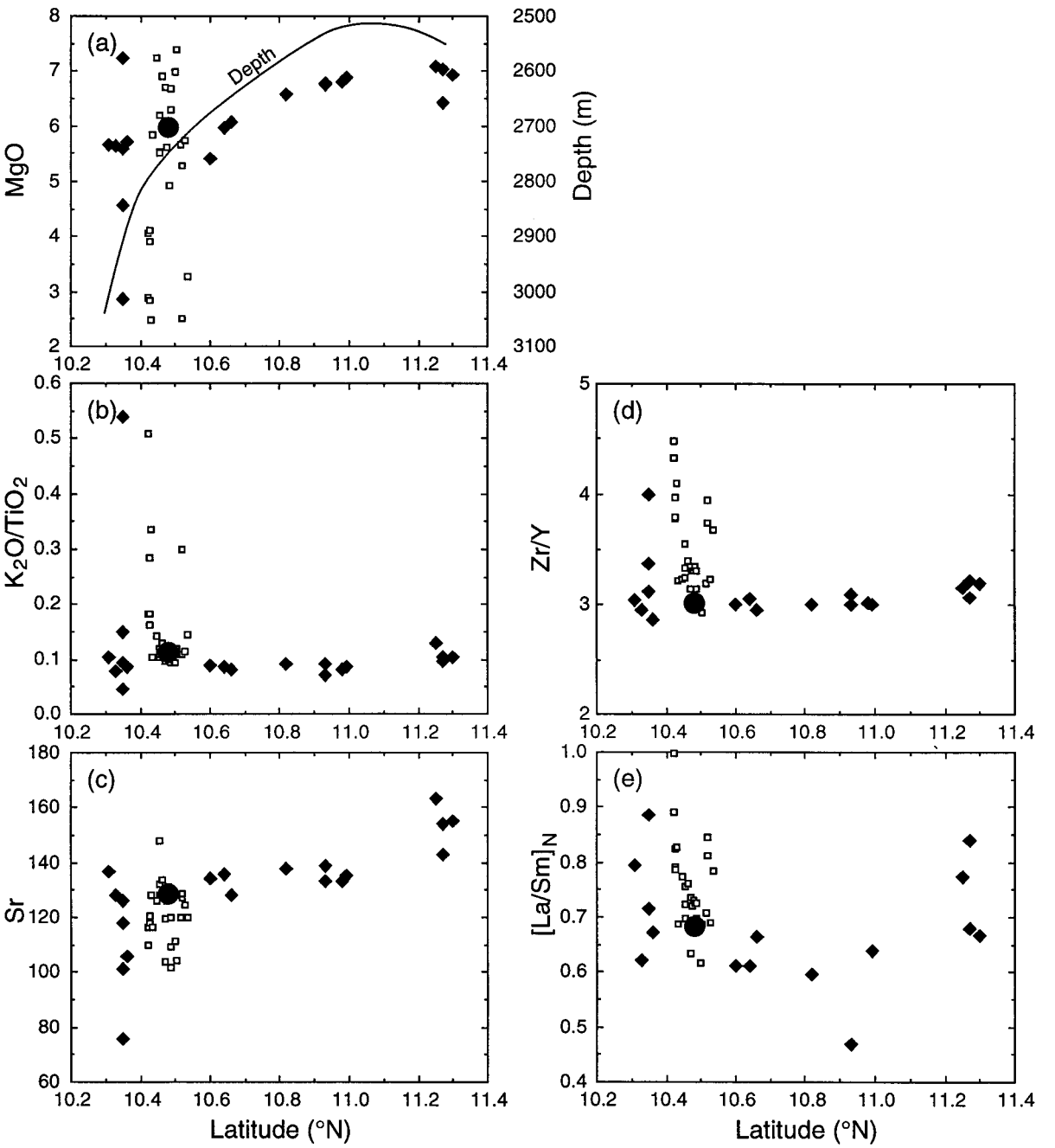

Fig. 7. Variation in (a) MgO, (b) K_2O/TiO_2, (c) Sr, (d) Zr/Y, and (e) $[La/Sm]_N$ with latitude for lavas from close to the EPR axis between the CFZ and 11°15′N (filled diamond symbols; data from Thompson et al. [5]), and samples dredged from off-axis at 10°30′N (squares). The average composition of samples from the neovolcanic zone (younger than 50 ka) at 10°30′N is also shown (filled circle). Note the systematic variation in the major and trace element chemistry of the young lavas from close to the ridge axis with latitude, which may indicate that a continuous melt lens underlies this ridge segment and is fed with melt beneath the topographic high near 11°N, close to where the least evolved lavas were erupted [5].

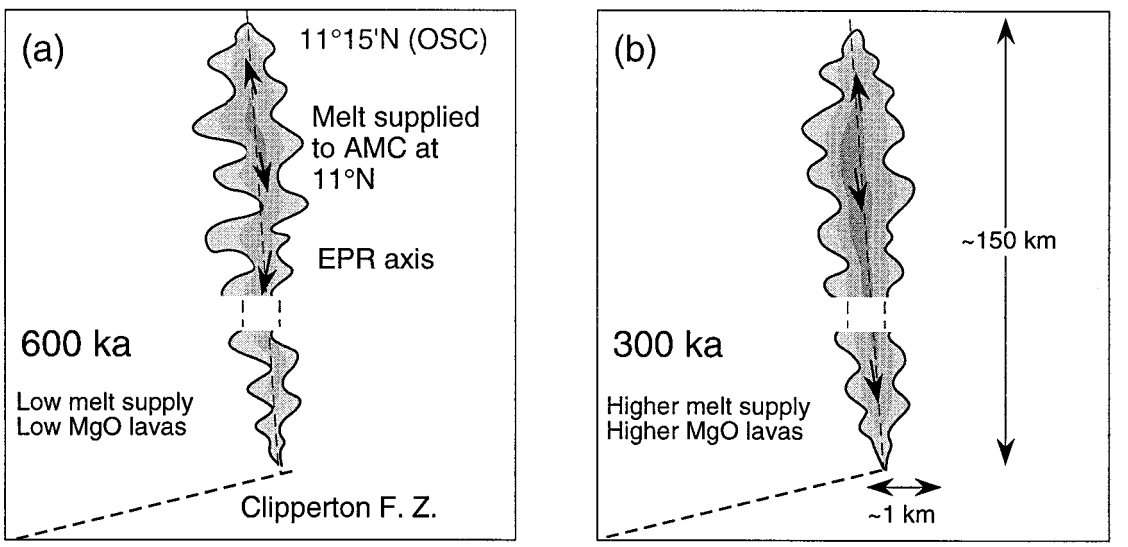

Fig. 8. Schematic plan section through the melt lens beneath the EPR between the 11°15′N OSC and the CFZ, to show the possible evolution of the magmatic plumbing system beneath this ridge segment. (a) At ~600 ka, the rate of magma supply to the melt lens beneath the topographic high near 11°N was relatively low, and relatively fractionated lavas were erupted from a narrow melt lens. The major element variation among lavas erupted within the neovolcanic zone may reflect cooling in melt 'lobes' which are partially isolated from the main melt lens. (b) By ~300 ka, an increase in the melt supply rate had led to development of a wider melt lens, erupting less fractionated lavas.

and along-axis transport of melt within a melt lens may be responsible for the along-axis variations in major and trace element chemistry of lavas erupted close to the ridge axis on this segment of the EPR.

As discussed in Section 6.1, variations in the rate at which melt is supplied to this melt lens result in variations in the major element chemistry of the lavas erupted at the ridge axis over periods of a few 100 ka. A number of different processes could lead to chemical variations on shorter timescales. For example, a recent U-series study of young lavas from the EPR near 9°30′N suggests that magmas have residence times in crustal magma chambers on the order of a few ka [48]. If such crustal residence times are generally applicable, this observation may explain some of the variation in incompatible trace element and isotope ratios seen in lavas dredged from off-axis at 10°30′N. Thus, at ~220 ka the melt lens may have been briefly filled with melt having relatively high Zr/Nb and low $^{87}Sr/^{86}Sr$, so that for a few ka, flows with compositions similar to that of 54-3 (Fig. 5) were erupted at the ridge axis. Alternatively, these 'anomalous' flows may result from off-axis eruptions of magmas that escaped mixing in the AMC.

Variations in the major element compositions of lavas erupted within the neovolcanic zone at 10°30′N could reflect the fine-scale structure of the melt lens. Previous studies have argued that the melt lens may have a 'lobed' structure [6,20], with the lobes having limited exchange with the main body of the melt lens (Fig. 8). Lobes a few 100 m across (volumes similar to the volume of individual flows) will have lifetimes of less than a few ka. Cooling and crystallization in semi-isolated magma bodies of this type could explain the major element variation observed in the core samples, which were erupted within the last 50 ka.

A similar model has been proposed for the 9°31′N region by Perfit et al. [20]. At this location, lavas from the axial summit caldera tend to have less chemical variation than lavas erupted outside the caldera, which led Perfit et al. to suggest that melts erupted at the ridge axis were derived from an axial magma chamber, whereas those erupted on the flanks within 4 km of the axis were derived from smaller magma bodies on the edges of a melt lens.

In the future, geophysical techniques may be able to resolve the small-scale variations in the shape

of the melt lens that we suggest are responsible for the short-term major element variations. Better constraints on the ages of lavas erupted within the neovolcanic zone using U-series methods, are also needed in order to determine the processes that are responsible for chemical variations that occur over periods of less than about 100 ka.

6.4. Magmatic 'cycles'?

Several authors have proposed that the chemistry of the lavas erupted on a single segment of the mid-ocean ridge system may change cyclically. The physical processes which might lead to cyclic variations in MORB chemistry are not fully understood, although it has been suggested that major melting events in the upper mantle may occur periodically in response to convective instabilities [7,44,49]. Such magmatic cycles have not yet been convincingly demonstrated, because so few studies of off-axis MORB have been carried out. Reynolds et al. [17] suggested that at 12°15′N, lava chemistry may vary cyclically with a period of around 300 ka. As discussed in Section 6.1, previous studies have attempted to explain structural changes in ridge segments as reflecting variable, cyclic magma supply to the ridge.

Our data show that at 10°30′N, the chemistry of lavas erupted at the ridge axis has varied considerably over the past 800 ka. These variations are not necessarily cyclic, although the changes in lava chemistry could be explained by cyclic magma recharge of the AMC with a period on the order of about 700 ka (Fig. 6). Shorter-period (150–350 ka) magmatic cycles have been inferred for this ridge segment from magnetic data [16]. Further studies of off-axis samples, extending to greater distances from the ridge axis, and at different locations on this ridge segment are needed in order to determine whether these variations in melt supply are indeed cyclic.

7. Conclusions

Glasses dredged from the flanks of the EPR, from up to 50 km from the ridge axis at 10°30′N can be used to examine temporal changes in the chemistry of lavas erupted at the ridge axis over the past 800 ka. The width of the neovolcanic zone appears to be less than 4 km, and thus the samples can be used to examine temporal changes in the average composition of lavas erupted at the ridge axis over periods of a few hundred thousand years. Changes in the average major element composition of lavas erupted at the ridge axis are related to changes in the rate at which melt is supplied beneath the ridge axis, supporting previous arguments that variations in melt supply rate are an important influence on the chemistry of lavas erupted over periods of a few hundred thousand years. However, the large temporal chemical variations on this ridge segment are unlikely to be typical of the EPR. Our data support previous evidence for systematic along-axis variations in the chemistry of young lavas from close to the ridge axis. These chemical variations are consistent with the presence of a melt lens beneath this ridge segment, which is fed by melt beneath the axial high near 11°N.

Samples younger than 50 ka, from within the neovolcanic zone at 10°30′N, have a smaller range in major element composition compared to samples dredged from the ridge flanks. On timescales of <50 ka, variations in the major element chemistry of lavas may be controlled by irregularities in the shape of the melt lens, where the cooling rate varies locally and magma mixing is incomplete. Occasional non-systematic variations in isotope and incompatible trace element ratios observed in the dredge samples could either reflect variations in the trace element chemistry of the melt that is supplied to the melt lens over periods of a few ka, or batches of melt which reach the surface without undergoing significant mixing and homogenization in the magma chamber.Table 1Major and trace element data for lavas from the East Pacific Rise at 10°30′N

Acknowledgements

This work was supported by grants from the Australian Research Council and The University of Queensland. We thank E.E.E. Hooft, M.R. Perfit, and an anonymous reviewer for their thorough and constructive reviews. ***[CL]***

References

[1] R.S. Detrick, P. Buhl, E. Vera, J. Mutter, J. Orcutt, J. Madsen, T. Brocher, Multi-channel seismic imaging of a crustal magma chamber along the East Pacific Rise, Nature 326 (1987) 35–41.

[2] G.M. Kent, A.J. Harding, J.A. Orcutt, Evidence for a smaller magma chamber beneath the East Pacific Rise at 9º30′N, Nature 344 (1990) 650–653.

[3] J.H. Natland, Effect of axial magma chambers beneath spreading centers on the compositions of basaltic rocks, DSDP Init. Rep. 54 (1980) 833–850.

[4] J.M. Sinton, R.S. Detrick, Mid-ocean ridge magma chambers, J. Geophys. Res. 97 (1992) 197–216.

[5] G. Thompson, W.B. Bryan, S.E. Humphris, Axial volcanism on the East Pacific Rise, 10–12ºN, in: A.D. Saunders, M.J. Norry (Eds.), Magmatism in the Ocean Basins, Geol. Soc. Spec. Publ. 42 (1989) 181–200.

[6] R. Batiza, Y. Niu, Petrology and magma chamber processes at the East Pacific Rise ~9º30′N, J. Geophys. Res. 97 (1992) 6779–6797.

[7] J.A. Whitehead, H.J.B. Dick, H. Schouten, A mechanism for magmatic accretion under spreading centers, Nature 312 (1984) 146–147.

[8] C.H. Langmuir, J.F. Bender, R. Batiza, Petrological and tectonic segmentation of the East Pacific Rise, 5º30′–14º30′N, Nature 322 (1986) 422–429.

[9] K.C. Macdonald, P.J. Fox, L.J. Perram, M.F. Eisen, R.M. Haymon, S.P. Miller, S.M. Carbotte, M.-H. Cormier, A.N. Shor, A new view of the mid-ocean ridge from the behaviour of ridge-axis discontinuities, Nature 335 (1988) 217–225.

[10] P. Lonsdale, Nontransform offsets of the Pacific–Cocos plate boundary and their traces on the rise flank, Geol. Soc. Am. Bull. 96 (1985) 313–327.

[11] Y. Niu, R. Batiza, An empirical method for calculating melt compositions produced beneath mid-ocean ridges: application for axis and off-axis (seamounts) melting, J. Geophys. Res. 96 (1991) 21753–21777.

[12] J.M. Sinton, S.M. Smaglik, J.J. Mahoney, Magmatic processes at superfast spreading mid-ocean ridges: glass compositional variations along the East Pacific Rise 13–23ºS, J. Geophys. Res. 96 (1991) 6133–6155.

[13] W. Bach, E. Hegner, J. Erzinger, M. Satir, Chemical and isotopic variations along the superfast spreading East Pacific Rise from 6º to 30º, Contrib. Mineral. Petrol. 116 (1994) 365–380.

[14] R. Batiza, Magmatic segmentation of mid-ocean ridges: a review, in: C.J. MacLeod, P.A. Tyler, C.L. Walker (Eds.), Tectonic, Magmatic, Hydrothermal and Biological Segmentation of Mid-Ocean Ridges, Geol. Soc. Spec. Publ. 118 (1996) 103–130.

[15] R. Hekinian, G. Thompson, D. Bideau, Axial and off-axial heterogeneity of basaltic rocks from the East Pacific Rise at 12º35′N–12º51′N and 11º26′N–11º30′N, J. Geophys. Res. 94 (1989) 17437–17463.

[16] S. Carbotte, K. Macdonald, East Pacific Rise 8º–10º30′N: evolution of ridge segments and discontinuities from SeaMARC II and three-dimensional magnetic studies, J. Geophys. Res. 97 (1992) 6959–6982.

[17] J.R. Reynolds, C.H. Langmuir, J.F. Bender, K.A. Kastens, W.B.F. Ryan, Spatial and temporal variability in the geochemistry of basalts from the East Pacific Rise, Nature 359 (1992) 493–499.

[18] R. Hekinian, D. Walker, Diversity and spatial zonation of volcanic rocks from the East Pacific Rise near 21ºN, Contrib. Mineral. Petrol. 96 (1987) 265–280.

[19] J.L. Karsten, J.R. Delaney, J.M. Rhodes, R.A. Liias, Spatial and temporal evolution of magmatic systems beneath the Endeavour Segment, Juan de Fuca Ridge: tectonic and petrologic constraints, J. Geophys. Res. 95 (1990) 19235–19256.

[20] M.R. Perfit, D.J. Fornari, M.C. Smith, J.F. Bender, C.H. Langmuir, R.M. Haymon, Small-scale spatial and temporal variations in mid-ocean ridge crest magmatic processes, Geology 22 (1994) 375–379.

[21] R. Batiza, Y. Niu, J.L. Karsten, W. Boger, E. Potts, L. Norby, R. Butler, Steady and non-steady state magma chambers below the East Pacific Rise, Geophys. Res. Lett. 23 (1996) 221–224.

[22] D.S. Stakes, J.W. Shervais, C.A. Hopson, The volcanic–tectonic cycle of the FAMOUS and AMAR valleys, Mid-Atlantic Ridge (36º47′N): evidence from basalt glass and phenocryst compositional variations for a steady-state magma chamber beneath the valley midsections, AMAR 3, J. Geophys. Res. 89 (1984) 6995–7028.

[23] M.C. Smith, M.R. Perfit, I.R. Jonasson, Petrology and geochemistry of basalts from the southern Juan de Fuca Ridge: controls on the spatial and temporal evolution of mid-ocean ridge basalt, J. Geophys. Res. 99 (1994) 4787–4812.

[24] M.L. Begnaud, J.S. McClain, G.A. Barth, J.A. Orcutt, A.J. Harding, Velocity structure from forward modelling of the eastern ridge-transform intersection area of the Clipperton Fracture Zone, East Pacific Rise, J. Geophys. Res. 102 (1997) 7803–7820.

[25] D.G. Gallo, P.J. Fox, K.C. Macdonald, A Seabeam investigation of the Clipperton Transform Fault: the morpho-tectonic expression of a fast slipping transform boundary, J. Geophys. Res. 91 (1986) 3455–3467.

[26] ARGO-RISE Group, Geological mapping of the East Pacific Rise axis (10º19′–11º53′N) using the ARGO and ANGUS imaging systems, Can. Mineral. 26 (1988) 467–486.

[27] K.C. Macdonald, P.J. Fox, The axial summit graben and cross-sectional shape of the East Pacific Rise as indicators of axial magma chambers and recent volcanic eruptions, Earth Planet. Sci. Lett. 88 (1988) 119–131.

[28] K.C. Macdonald, Tectonic and magmatic processes on the East Pacific Rise, in: E.L. Winterer, D.M. Hussong, R.W. Decker, (Eds.), The Eastern Pacific Ocean and Hawaii: The Geology of North America, Vol. N, Geological Society of America, Boulder, CO, 1989, pp. 93–110.

[29] E.E.E. Hooft, R.S. Detrick, G.M. Kent, Seismic structure and indicators of magma budget along the southern East Pacific Rise, J. Geophys. Res. 102 (1997) 27319–27340.

[30] G.A. Barth, J.C. Mutter, Variability in oceanic crustal thickness and structure: multichannel seismic reflection results from the northern East Pacific Rise, J. Geophys. Res. 101 (1996) 17951–17975.
[31] Y. Niu, R. Batiza, Trace element evidence from seamounts for recycled oceanic crust in the eastern equatorial Pacific mantle, Earth Planet. Sci. Lett. 148 (1997) 471–484.
[32] S.J. Goldstein, M.R. Perfit, R. Batiza, D.J. Fornari, M.T. Murrell, Off-axis volcanism at the East Pacific Rise based on uranium-series dating of basalts, Nature 367 (1994) 157–159.
[33] K.C. Macdonald, P.J. Fox, R.T. Alexander, R. Pockalny, P. Gente, Volcanic growth faults and the origin of Pacific abyssal hills, Nature 380 (1996) 125–129.
[34] R.A. Duncan, L.G. Hogan, Radiometric dating of young MORB using ^{40}Ar–^{39}Ar incremental heating method, Geophys. Res. Lett. 21 (1994) 1927–1930.
[35] D.J. Fornari, M.R. Perfit, A. Malahoff, R. Embley, Geochemical studies of abyssal lavas recovered by DSRV Alvin from eastern Galapagos Rift, Inca Transform, and Ecuador Rift, 1, Major element variations in natural glasses and spacial distribution of lavas, J. Geophys. Res. 88 (1983) 10519–10529.
[36] W.W. Chadwick Jr., R.W. Embley, Lava flows from a mid-1980s submarine eruption on the Cleft segment, Juan de Fuca Ridge, J. Geophys. Res. 99 (1994) 4761–4776.
[37] J.M. Sinton, D.S. Wilson, D.M. Christie, R.N. Hey, J.R. Delaney, Petrologic consequences of rift propagation on oceanic spreading centers, Earth Planet. Sci. Lett. 62 (1983) 193–207.
[38] C.H. Langmuir, J.F. Bender, The geochemistry of oceanic basalts in the vicinity of transform faults: observations and implications, Earth Planet. Sci. Lett. 69 (1984) 107–127.
[39] E.M. Klein, The Clipperton Transform Team, The CHEPR Team, Geochemistry of basalts collected during Alvin dives within and adjacent to the Clipperton Transform Fault (19ºN East Pacific Rise), Eos 68 (1987) 1540.
[40] G.A. Barth, K.A. Kastens, E.M. Klein, The origin of bathymetric highs at ridge-transform intersections: a multi-disciplinary case study at the Clipperton Fracture Zone, Mar. Geophys. Res. 16 (1994) 1–50.
[41] K. Harpp, W.M. White, R. Batiza, Isotopic study of contrasting magmatic suites: The East Pacific Rise at 9º30′N and the MAR in the FAMOUS area, Eos 71 (1990) 658.
[42] M.C. Smith, M.R. Perfit, R.W. Embley, W.W. Chadwick, Interpretation of magmatic activity and crustal accretion along the CoAxial segment and Axial Seamount North Rift zone: using combined acoustic and geochemical data to map the seafloor at the scale of individual flows, Eos 78 (1997) F676.
[43] D.M. Christie, J.M. Sinton, Evolution of abyssal lavas along propagating segments of the Galapagos spreading center, Earth Planet. Sci. Lett. 56 (1981) 321–335.
[44] D.S. Scheirer, K.C. Macdonald, Variation in cross-sectional area of the axial ridge along the East Pacific Rise: evidence for the magmatic budget of a fast spreading center, J. Geophys. Res. 98 (1993) 7871–7886.
[45] K. Crane, The spacing of ridge axis highs: dependence upon diapiric processes in the underlying asthenosphere, Earth Planet. Sci. Lett. 72 (1985) 405–414.
[46] L.J. Perram, K. Macdonald, A one-million year history of the 11º45′N East Pacific Rise discontinuity, J. Geophys. Res. 95 (1990) 21363–21381.
[47] D.J. Fornari, D.G. Gallo, M.H. Edwards, J.A. Madsen, M.R. Perfit, A.N. Shor, Structure and topography of the Siqueiros transform fault system: evidence for the development of intra-transform spreading centers, Mar. Geophys. Res. 11 (1989) 263–299.
[48] K.W.W. Sims, S.J. Goldstein, D.J. Fornari, M.T. Murrell, M. Perfit, S.R. Hart, U-series analyses of young lavas from 9–10ºN East Pacific Rise: constraints on magma transport and storage times beneath the ridge axis (abstr.), Eos 78 (1997) F792.
[49] H. Schouten, K.D. Klitgord, J.A. Whitehead, Segmentation of mid-ocean ridges, Nature 317 (1985) 225–229.